Effect of sawtooth crashes on fast-ion distribution in NSTX-U

D. Liu[1], W. W. Heidbrink[1], M. Podestà[2],G. Z. Hao[1],D. S. Darrow[2], E. D. Fredrickson[2] and D. Kim[2]

[1] *Department of Physics and Astronomy, University of California-Irvine, Irvine, CA 92697, USA*

[2] *Princeton Plasma Physics Laboratory, Princeton, NJ 08543, USA*

Abstract.

During the 2016 experimental campaign of NSTX-Upgrade (NSTX-U), long L-mode and reproducible sawtoothing plasmas have been achieved that were previously not accessible before the upgrade. This provides a good opportunity to study the effect of sawtooth crashes on fast ion confinement and re-distribution in spherical tokamaks. The Solid State Neutral Particle Analyzer (SSNPA) and Fast-Ion D-alpha (FIDA) diagnostics on NSTX-U each have a tangentially-viewing instrument and a radially- or vertically-viewing instrument, which are mainly sensitive to passing and trapped fast ions respectively. It has been observed on both diagnostics that passing particles are strongly expelled from the plasma core to the edge during sawtooth crashes, while trapped fast ions are weakly affected. The tangential-viewing SSNPA observes large signal spikes at the sawtooth crashes because fast ions move to the edge and charge exchange with edge neutrals. The radially-viewing SSNPA data suggest that there is a small drop of trapped particles in the core. The tangential-viewing FIDA system observes a depletion as large as 25% in the region inside the inversion radius, while an increase at the outer region. There is almost no change in the signals of the vertically-viewing FIDA system. The neutron emission can drop as much as 15% at the sawtooth crashes, accompanied by an increase of edge $D_\alpha$light. Simulations with the Kadomstev and Porcelli sawtooth models have been performed and compared with measurements. The standard Kadomtsev model overestimates the neutron rate drop at each sawtooth crash. The Porcelli sawtooth model can qualitatively reproduce the neutron rate drop and FIDA signal drop in the core, but fails to predict the FIDA signal increase at the edge.

1. Introduction

Sawtooth crashes are periodic collapses of central plasma temperature followed by slow recoveries when the safety factor q at the magnetic axis, q_0, drops below unity. After it was first discovered by Von Goeler et al. in 1974[1], sawtooth crashes have been observed in nearly every tokamak device. Sawtooth crashes can cause significant transport of bulk plasma and fast ions from neutral beam injection or RF heating. Large sawtooth crashes can trigger neoclassical tearing modes[2], which may degrade the plasma confinement and lead to a plasma disruption. On the other hand, the redistribution of the fast ions could also change their interaction with the background plasma, and thus affect fast-ion confinement and MHD instabilities, including the sawtooth itself. It is important to understand the effect of sawtooth crashes on the fast ion population and develop a coherent sawtooth control strategy to take account of the alpha particles and fast ions from auxiliary heating systems. In this paper, we mainly focus on the effect of sawtooth crashes on the fast ion distribution.

Recent experiments on TEXTOR[3], DIII-D[4], and ASDEX Upgrade[5, 6, 7] show that in conventional tokamaks passing fast ions are much more susceptible to sawtooth-induced transport than trapped particles. The DIII-D experimental data also suggest that the redistribution of fast ions may have some energy dependence. All these observations qualitatively agree with the Kadomstev sawtooth model[8, 9]. In the Kadomstev model, a sawtooth crash is essentially a magnetic reconnection process in which a fast change of helical magnetic flux and a large electric field are induced. The simulations with the Kadomstev model reproduce the trend observed in experiments, but there is some discrepancy in the magnitude of the change[4]. However, the effect of sawtooth crashes on the fast-ion distribution in spherical tokamaks is much less studied. In principle, sawteeth in spherical tokamaks could be significantly different from those in conventional tokamaks. Because of the relatively low magnetic field, fast ions from neutral beam injection in spherical tokamaks have very large gyro-orbit width. For example, ρ/a in the spherical tokamak NSTX[10] can be as large as 0.3 for typical beam injection energies of $80-90$ keV, where ρ is the fast ion gyroradius radius and a is the minor radius. Moreover, the ratio

of beam ion gyroradius to machine size in the existing spherical tokamaks is comparable to the ratio of alpha-particle gyroradius to machine size in future spherical tokamak D-T reactors. In addition, spherical tokamaks generally have higher values of β (the ratio of bulk plasma pressure to the magnetic field pressure) and a larger population of fast ions compared with conventional tokamaks. Therefore, the sawtooth studies in spherical tokamaks can complement the studies in conventional high field tokamaks and help with sawtooth model development and code validation.

The National Spherical Torus eXperiment Upgrade facility (NSTX-U)[11, 12, 13] is a mid-size spherical tokamak with toroidal field $B_T(0)$ up to 1 T, plasma current of $I_p = 1.0 - 2.0$ MA and aspect ratio $R/a = 1.6 - 1.8$. The NSTX-U completed its first plasma operation campaign[14] in the summer of 2016 after it completed two main upgrades from NSTX[10]: (1) a new and larger center stack that can approximately double the toroidal magnetic field and plasma current, and (2) the addition of three outboard neutral beam sources with $R_{tan} = 1.3, 1.2,$ and 1.1 m (labeled $2A$, $2B$, and $2C$, respectively) in addition to the existing three inboard neutral beam sources from NSTX with tangency $R_{tan} = 0.7$, 0.6, and 0.5 m, (labeled $1A$, $1B$, and $1C$, respectively), as shown in Fig. 1. These three new outboard beam sources aim at increasing the available auxiliary heating power and neutral beam driven current and expanding the flexibility in fast ion pressure, rotation and q profile control. The total neutral beam injection power is increased from 6 MW to 10 MW. In the NSTX-U's 2016 campaign, 2-sec long L-mode sawtooth discharges that had not been available on NSTX were routinely achieved. Although the sawtoothing discharges in this paper are obtained from the NSTX-U commissioning phase, the main fast ion diagnostics that will be described in Section 2 already worked properly. These sawtooth shots provide a good database to study the effect of sawtooth crashes on fast ion distribution in spherical tokamaks.

The paper is organized as follows. The plasma conditions and main fast ion diagnostics will be firstly described in Section 2. Then the experimental setup and fast-ion diagnostic measurements during the sawtooth crashes will be presented. Measurements from multiple fast ion diagnostics confirm that sawtooth crashes affect passing and trapped fast ions differently. Section 3 compares the TRANSP[15, 16] sawtooth simulations with experimental measurements. Standard Kadomstev

model and Porcelli model[17] have been used in the simulations. In addition, the critical energies for redistribution of passing and trapped fast ions based on Kolesnichenko's theory[18, 19, 20] are calculated. They can explain the experimental observations reasonably well. Finally, Section 4 summarizes the conclusions of this study and on-going work.

2. Experimental setup and measurements

The fast-ion distribution function is a complicated function in phase space. Its deposition requires at least two dimensions in real space and two dimensions in velocity/energy. Therefore, multiple diagnostics are often needed to diagnose the fast-ion distribution. The fast ion diagnostic suite on NSTX-U consists of neutron detectors, Solid State Neutral Particle Analyzer (SSNPA) arrays[21, 22] and Fast-Ion D-alpha (FIDA) spectroscopy[23, 24]. A scintillator-based Fast Loss Ion Probe (sFLIP)[25, 26] and a charged fusion product diagnostic[27, 28] are also planned for NSTX-U and will be available in the future. The neutron detectors measure the volume-integrated neutron flux. They provide a good indicator of high energy fast ions in the plasma core since beam-target reaction is the dominant fusion reaction on NSTX-U.

Figure 1 shows the SSNPA and FIDA detector locations and sightlines projected onto the equatorial plane of the NSTX-U vessel. The newly developed SSNPA diagnostic is a compact solid state Neutral Particle Analyzer (NPA) based on silicon photodiodes. It measures fast re-neutrals that escape from the plasma through a Charge Exchange (CX) reaction of a fast ion with a neutral particle. The escaping velocity is determined by the fast-ion velocity at the time of the CX reaction. Consequently, each NPA detector measures a narrow range of velocity pitch angles with respect to the magnetic field. These localized measurements in phase space are a valuable complement to techniques that average over pitch angles, such as neutron and FIDA diagnostics. The CX reactions are either with neutrals from neutral beam injection or with cold neutrals that penetrate into the plasma from the edge. The former process is called active CX, while the latter is called passive CX. The SSNPA instrument on NSTX-U consists of three 16-channel silicon photodiode arrays stacked vertically. The photodiodes are operated in current mode for high temporal resolution. To

obtain some energy resolution, the three arrays are coated with thin foils of different thickness; energy loss in the foils determines the minimum energy detected in each array. To obtain a spatial profile from active charge-exchange measurements, the sightlines of the arrays are oriented to intersect a heating neutral beam. One instrument, labeled t-SSNPA, is oriented to measure ions with large tangential velocity components and has sightlines that intersect the more tangential $2A$, $2B$, and $2C$ sources. Another instrument, named r-SSNPA, is oriented to measure neutrals with large radial velocity components and has sightlines that intersect the more perpendicular $1A$, $1B$, and $1C$ sources. In addition, a similar instrument with only one silicon photodiode array is oriented radially with sightlines that miss all heating beams; it monitors the passive signal and is called p-SSNPA. The SSNPA diagnostic worked very well on NSTX-U, and it can detect fluctuations up to 120 kHz with a sampling rate of 500 kHz. The energy threshold for the three different thickness filters are > 25 keV, > 45 keV, and > 65 keV respectively.

The FIDA diagnostic is an application of charge-exchange recombination spectroscopy[29]. It measures the Doppler-shifted D_α emission of re-neutralized fast deuterons which have undergone CX reaction with beam neutrals or background neutrals. The light is collected by optical fibers and then sent to a spectrometer, and spectral resolution is obtained by dispersion of a bandpass-filtered portion of the light. The spectrum of FIDA light provides useful information about the distribution of fast ion velocity along the sightline. To get the FIDA spatial profile, FIDA spectra from each radial sightline are integrated over a particular wavelength range of interest. Similar to the SSNPA diagnostic, FIDA light can come from active signals when the CX reaction is with injected beam neutrals, and from passive signals when the CX reaction is with background neutrals, especially edge neutrals. There are currently two sets of FIDA diagnostics on NSTX-U: a toroidally viewing FIDA (labeled t-FIDA) from a lens mounted slightly above the vessel midplane, and a vertically viewing FIDA (named v-FIDA) from two lenses mounted on the top of the machine that look vertically downwards at the centerline of neutral beam source $1B$. Both FIDA systems have 16 active fibers, and the intersectional points with the centerline of neutral beam source $1B$ are nominally the same for the t-FIDA and v-FIDA systems. The 16 fibers cover the whole plasma

region from $R_{maj} = 85cm$ to $R_{maj} = 155cm$, where R_{maj} is the major radius at which the sightlines intersect the neutral beam. The spatial resolution of the FIDA diagnostic is about 5 cm and the temporal resolution is 10 ms. Background subtraction is critical for the FIDA diagnostic. Each FIDA system has 16 toroidally-displaced passive (or reference) views to monitor background or passive emissions. It has also been recently observed that scattered cold D_α light in the optical system or inside the vacuum vessel can contaminate the baseline of the FIDA spectra[30]. A scattering correction[30] based on singular value decomposition (SVD) has been employed in all FIDA data shown in this paper.

The sawtooth events analyzed in the paper are obtained from NSTX-U deuterium discharges with a flat-top plasma current of $I_p = 700$ kA and a toroidal magnetic field of 0.65 T at the magnetic axis ($R_0 \simeq 1.05$ m). These discharges are low density L-mode discharges which are very suitable for FIDA and SSNPA diagnostic measurements. Figure 2 shows the spectrogram of Mirnov coil signals and time traces of injected neutral beam power and neutron rate in a typical sawtooth discharge with shot number 204163. Only neutral beam source $1B$ is used to heat the plasma. The injected neutral beam power is $P_{inj} = 1.1$ MW with energy of $E_{inj} = 72$ keV. The core electron density and temperature are of order of $2.0 \times 10^{19} cm^{-3}$ and 1.5 keV respectively. The discharge has repetitive sawtooth crashes between 0.5 and 1.5 s. Although the Motional Stark Effect (MSE) diagnostic was not available for q-profile measurement, the instabilities are identified as sawtooth crashes based on two facts: (1) the electron temperature is observed by the multi-point Thompson scattering and x-ray diagnostics to be flattened in the plasma core after the crash; and (2) there are $n = 1$ signals in Mirnov spectrogram where n is the toroidal mode number.

Figure 3 shows the temporal evolution of key plasma parameters related to the fast ion population and MHD activity in the discharge 204163. As shown in Fig. 3(b), a sawtooth crash can result in as large as a 15% drop of the neutron yield, implying a significant fast ion redistribution or fast ion losses. The D_α radiance from the edge of the plasma also shows a spike right after every sawtooth crash. The spikes in D_α light is hypothesized to be the result of CX reactions between thermal or fast ions that are ejected from the plasma by the sawtooth and neutrals near the plasma

boundary. Both the SSNPA and FIDA diagnostics have observed clear effects of sawtooth crashes on the fast ions. The effect of individual sawtooth events on the SSNPA signals is readily seen in the time traces in Fig. 3(c)-(e). The p-SSNPA, mainly sensitive to passive signals from trapped particles at the edge, observes a small signal increase at each sawtooth crash. The t-SSNPA, mainly sensitive to passive signals from passing particles near the edge, observes a big spike at each sawtooth crash. This is likely because passing fast ions are redistributed to the edge and charge exchange with edge neutrals. The r-SSNPA views the heating beam $1B$, and the signal is the combination of active signal from the core and passive signal from the edge. The r-SSNPA signal shows a small depletion at each sawtooth crash. Considering that the passive signal from trapped particles slightly increases at each sawtooth crash as indicated by Fig. 3(c), the active signal of r-SSNPA from trapped particles is inferred to drop at the sawtooth crash.

All the sawtooth events in the discharge 204163 between 0.5 and 1.5 s are combined into one database to quantify the correlation between the SSNPA signal change and neutron rate drop at sawtooth crashes. Because the neutron emission in NSTX-U is dominated by beam-plasma reactions, the drop of the neutron rate is used as an indictor of how fast ions are affected by sawteeth. As shown in Fig. 4, the change of the p-SSNPA signal follows the same trend as the edge D_α signal, which suggests that the change of the p-SSNPA signal is mainly due to the change of edge neutral density. Please note that the SSNPA signal is the line integral of the product of fast ion density and neutral density along the sightline. The p-SSNPA does not intersect with any neutral beam footprint. The signal mainly comes from the edge simply because the neutral density is orders of magnitude higher in the edge than in the plasma core. Figure 4 clearly shows that the t-SSNPA signal increases rapidly with the neutron rate drop. The t-SSNPA signal can increase as much as a factor of 2 when the neutron rate drop is close to 15%. Since the change of the t-SSNPA signal is one order of magnitude larger than the change of D_α, it suggests that passing fast ions are strongly expelled from the core to the edge. It should be noted that the t-SSNPA also does not intersect with any neutral beam in this case and its signal is mainly from the passing fast ions near the edge. One valuable feature of the SSNPA diagnostic on NSTX-U is that there are

three vertical stacked arrays viewing the similar plasma region with different filter thickness. This setup makes the SSNPA have not only fast ion temporal resolution but also some coarse energy information. It is interesting to observe that all the arrays of t-SSNPA have the same trend, which suggests that a wide energy range of passing fast ions are affected by the sawtooth. In contrast, the r-SSNPA observes a small signal drop, which indicates there actually is some depletion of trapped particles in the plasma core. There are at least 15 low-density L-mode discharges showing similar observations as the typical case shown above.

The effect of individual sawtooth crashes on the active FIDA signal is blurred by imperfect background subtraction because of large passive contribution, cold $D_\alpha$light scattering inside the FIDA optical system and possible light reflection and scattering from the NSTX-U in-vessel tiles[30]. Conditional averaging over several sawtooth events is employed to extract useful information from the relatively noisy FIDA data. Figure 5 (a) and (b) compare the active t-FIDA spectra before and after the sawtooth crash for two channels with $R_{maj} = 108$ cm and $R_{maj} = 135$ cm, where R_{maj} is the major radius that the t-FIDA sightline intersects with the neutral beam centerline. The active FIDA signal is obtained by subtracting the signal in the reference view from the signal in the active view. This removes the contribution from passive FIDA light and bremsstrahlung emission. The FIDA light part is the Doppler-shifted region in the spectra with wavelength from 650.35 nm to 653.4 nm, where the corresponding fast-ion energies parallel to the sightline are 72 keV and 10 keV respectively. As shown in Fig. 5 (a) and (b), the t-FIDA signal has a depletion in the core channel, but an increase at the outer channel. The whole detectable energy range is affected. Figure 5 (c) compares the t-FIDA spatial profile before and after the sawtooth, and Fig. 5 (d) shows the change of t-FIDA signals. A significant reduction occurs inside $R_{maj} = 125$ cm and an increase occurs in the t-FIDA outer channels. It is worthy to mention that the sawtooth inversion radius is about 120 cm and sawtooth crash time is typically around $40\mu s$ based on the soft x-ray data. For the v-FIDA system, little change is observed in the FIDA spectra before and after the sawtooth crash and the data are not shown. The changes on t-FIDA and v-FIDA signals before and after the sawtooth crash confirm the SSNPA observations that passing

particles are strongly redistributed from the core to the edge, while trapped particles are little or not affected.

Data from the innermost and outmost channels of the t-FIDA arrays are omitted in Fig. 5. After background subtraction, channels at the edge of the array have unphysical negative values. Generally on NSTX-U, these edge channels are more prone to background errors than the central chords. Although the data shown in Fig. 5 appear reasonable, it is possible that an unidentified error in background subtraction also affects the central channels; this would cause an unidentified offset in Fig. 5 (d)

Based on the above measurements from neutron, SSNPA and FIDA diagnostics, we can conclude that under the conditions studied here: (1) passing fast ions are strongly expelled from the core to the edge at each sawtooth crash, while trapped fast ions are weakly affected. (2) no clear energy dependence is observed in the redistribution of passing fast ions. These observations are very similar to the phenomenon detected in conventional tokamaks although sawtooth behavior in spherical tokamak and conventional tokamak could be different in principle. A strong effect of sawteeth on passing fast ions and a weak/negligible effect on trapped fast ions was observed on TEXTOR with the collective Thomson scattering diagnostic [3], on DIII-D with FIDA diagnostic [4], and ASDEX-Upgrade with FIDA and collective Thomson scattering measurements [5, 6, 7]. Sawteeth have also been observed to redistribute passing fast ions by neutron camera, charged fusion product and FIDA diagnostics in MAST[31], which is another spherical tokamak in the United Kingdom.

In addition to repetitive sawtooth discharges, there are some other interesting observations. As shown in Fig. 6, the sawtooth crashes almost disappear when the most perpendicular and most tangential beam alternatively is injected into the plasma. There is no obvious neutron rate drop and TRANSP predicted neutron emission is very close to the measurement. There are also no big spikes or drops on all the SSNPA arrays. The neutron and SSNPA data suggest that fast ions transport is strongly reduced. Many experimental and theoretical studies suggest that in conventional tokamaks, sawtooth behavior can be altered either by modifying the magnetic shear

at the resonance surface with safety factor $q = 1$ or by acting on the local fast ion distribution[32]. In addition, rotation can also change the sawtooth stability. It is not clear which factor plays the most important role here because it was in the commissioning phase and the MSE diagnostic was not available. A more careful check on this topic is left for future work.

3. Modelling of sawtooth and comparison with experiments

The time-dependent Tokamak transport code TRANSP[15, 16] is used to simulate sawtooth crashes and calculate the fast ion distribution before and after the sawtooth crashes. The time slices when the sawtooth events occur are specified in an input file. The sawtooth model used in TRANSP can be either the standard Kadomtsev model[8, 9] (with $NMIX\_KDSAW = 1$ in the TRANSP namelist) or Porcelli sawtooth model[17] (with $NMIX\_KDSAW = 3$ in the TRANSP namelist). The standard Kadomtsev model treats the sawtooth as an "internal disruption" resulting from the nonlinear growth of the $n = 1$ kink instability. The flux surfaces with equal helicity on the opposite sides of the $q = 1$ surface reconnect and form a new unified surface with $q(0) = 1$ and $q(r) > 1$. The internally calculated plasma equilibrium is self-adjusted at these time slices; and the current and pressure profiles are flattened within the mixing radius. Fast ions are also redistributed so that their density within the mixing radius is spatially uniform after the sawtooth. All the fast ions and thermal ions participating in the mixing are conserved. The Porcelli sawtooth model is a modified Kadomtsev model. The magnetic q at the magnetic axis rises only part of the way to unity. The magnetic reconnection is partial or incomplete. In the Porcelli sawtooth model, the island width fraction can be specified with the variable $FPORCELLI$ in the namelist.

A series of TRANSP runs have been performed for the typical NSTX-U sawtooth discharge 204163. Anomalous fast ion diffusion is turned off because no other significant instabilities are present in the time window between 0.5 and 1.5 s. The TRANSP runs are provided with EFIT equilibrium reconstructions and spline fits to experimental plasma profiles. The input experimental profiles are conditionally averaged respectively over all the sawtooth events by aligning them to a single crash time and normalizing them to their value before the sawtooth event. It is assumed that

each plasma parameter has a similar temporal evolution for all sawtooth crashes in a short time window just before and after each sawtooth crash. A conditional averaging is needed here because the raw experimental data do not have sufficient temporal resolution for accurate time-dependent sawtooth modelling. The electron density and temperature obtained from the multi-point Thomson scattering (MPTS) diagnostic have a time resolution of 16.6 ms. The ion density, temperature and toroidal rotation from the charge-exchange recombination spectroscopy (CHERS) diagnostic typically have a time resolution of 10 ms. After conditional averaging, the experimental plasma profiles are re-sampled on the 1 ms time scale for sawtooth simulation. Figure 7 shows that the plasma density and temperature evolve substantially during a sawtooth cycle. In principle, the rapid change of plasma profile especially plasma density can affect the neutron emission since the beam-target fusion reaction is proportional to the product of fast ion density and thermal ion density. The first TRANSP/NUBEAM run is used to check how much change of neutron emission is due to thermal plasma profile evolution. The sawtooth model is turned on for the q-profile evolution, but the effect of sawtooth crashes on the fast ion distribution is turned off. Figure 8 (a) shows that, as expected, there is little modulation in the fast ion density profile. It is a little bit surprising to notice that the neutron rate drop caused by thermal plasma profile evolution can be as large as 50% of the measured neutron rate drop at a sawtooth crash, see Fig. 8 (b) and (c). In the second TRANSP run, the standard Kadomtsev sawtooth model is turned on for both equilibrium and fast ions. As suggested in Fig. 9, the standard Kadomstev model overestimates the neutron rate drops at each sawtooth crash. Even when the fraction of fast ions participating in the sawtooth mixing ($XSWFRAC\_BEAM$ in the TRANSP namelist) is reduced from 1.0 to 0.5, the predicted neutron emission drop at the sawtooth crash is still about as twice as large as the experimental data.

Here, it should be noted that the magnitude of the neutron rate from the TRANSP simulation is re-scaled by a factor of 0.61 to match the experimental data before $t = 0.5$ s. The discrepancy in the absolute value also exists in the fast-ion confinement experiments in relatively quiescent plasmas with short beam blips. The discrepancy is partially because of uncertainty in the absolute calibration of the neutron detectors and partially because of the large uncertainty in the effective

charge Z_{eff} in TRANSP inputs. The same re-scaling factor is used in the rest of this paper.

In the third TRANSP simulation, the Porcelli sawtooth model is applied. As shown in Fig. 10, good agreement can be obtained between predicted and measured neutron rate when the following settings, $NMIX\_KDSAW = 3$, $FPORCELLI = 0.75$ and $XSWFRAC\_BEAM = 0.75$, are used. Here $NMIX\_KDSAW = 3$ is to select the Porcelli swtooth model, $FPORCELLI$ is the $q = 1$ island fraction, and $XSWFRAC\_BEAM$ is the fraction of fast ions involving in sawtooth mixing. In this case, the TRANSP calculated neutron rate overlaps with the experimental data and the neutron rate drops at the sawtooth crashes agree with experimental measurements. The redistribution of fast ion density especially in the core region is also obvious, see Fig. 10 (a). It should be mentioned that the global neutron emission seems not very sensitive to some settings. For example, when the fraction of reconnection ($FPORCELLI$) is changed from 1.0 to 0.5, the change of the drop of neutron emission at the sawtooth crash is less than 10%. In the TRANSP simulation, the NUBEAM module is called to calculate and dump out the fast-ion distribution every 2 ms in the time windows with sawtooth crashes. Figure 11 (a) shows the difference of the spatial distribution of fast ions before and after the sawtooth crash at $t = 0.643s$. It shows a strong reduction (20%) of fast ion density inside the sawtooth inversion radius and a modest increase (5%) at the edge. Figure 11 (b) compares the fast ion density as a function of energy before and after the sawtooth crash. It indicates that passing fast ions, which have large pitch, are strongly affected although TRANSP/NUBEAM treats all the fast ions and thermal ions the same way. This is mainly because the fast ions in the core region are dominated by passing fast ions. With the fast ion distributions from the TRANSP simulation, FIDAsim[33] code is used to calculate synthetic FIDA signal before and after the sawtooth. As shown in Fig. 12, the simulated t-FIDA signals after the sawtooth in most channels except the two edge channels are lower than the signals before the sawtooth crash. It is obvious that the FIDASIM simulation results are not entirely consistent with the FIDA experimental measurements: although they predict the depletion of FIDA signals in the core region, they fail to predict the signal increase at the edge. The experimental t-FIDA data in Fig. 5 show that the FIDA signal increases after the sawtooth at edge channels. This

discrepancy may reflect the limits of the Porcelli model in TRANSP. One of the main caveats of Kadomtsev and Porcelli models implemented in the TRANSP code is that they treat all the fast ions and thermal ions the same way and they do not include the kinetic effects of fast ions. In other words, fast particles are always attached to a magnetic flux surface, and the fast ions are redistributed according to the rearrangement of flux surfaces at the sawtooth crash. Thus, there is no energy or pitch dependence. Early simulations[34] have shown that full orbit effects may play an important role in a low magnetic field because the cyclotron resonances can enhance the level of stochasticity in fast ion orbits, thereby increasing the extent to which the fast ions are redistributed. In addition, other transport mechanisms, such as the resonant interaction between fast ions and the electromagnetic fields of the sawteeth[35, 36], can also affect fast ions during sawtooth.

According to the sawtooth theory in Ref. [18, 19], there are three characteristic time scales that determine the property of fast ion transport during a sawtooth crash: (1) the crash duration τ_{cr}; (2) the toroidal precession time τ_{pr}; and (3) longitudinal motion time τ_L which is the period around the perturbed the flux surface. The toroidal precession tends to keep the particles at a constant minor radius through de-correlation of the particle motion from the sawtooth and phase mixing. The longitudinal motion tends to move the particles along the displaced flux surfaces. If the sawtooth crash is sufficiently fast ($\tau_{cr} << \tau_{pr}$), fast ions move together with the evolving flux surfaces, and this leads to significant fast ion transport. However, when $\tau_{pr} < \tau_{cr}$, the influence of sawtooth crash on a particle's dynamics depends on the competition of τ_{pr} and τ_L. Strong fast ion transport can still occur when $\tau_{pr} >> \tau_L$. The conditions for strong redistribution are $\tau_{cr} << \tau_{pr}$ and $\tau_L << \tau_{pr}$, and they can be expressed in energy and pitch. In other words, there exists a pitch-dependent critical energy E_{crit}. The particles with energy less than E_{crit} are strongly redistributed at the sawtooth crash. For the discharge 204163 shown in this paper, the critical energies for passing and trapped particles are 65 and 15 keV respectively. The calculation of E_{crit} qualitatively reproduce the observed results that a large population of passing particles are strongly redistributed by sawteeth and that trapped particles are weakly affected.

4. Summary

Repetitive sawteeth are observed in long L-mode discharges on the NSTX-U in the 2016 run campaign. These sawtooth crashes can result in neutron rate drops as large as 15%, followed by an increase of edge $D_\alpha$light. The temporal evolution of plasma profiles can account for as much as 50% of the measured neutron rate drop at the sawtooth crash. Changes of fast ion diagnostic signals are strongly correlated with the sawtooth events. Analysis of the signal changes of three SSNPA instruments shows that passing fast ions in the whole detectable energy range are strongly redistributed from the plasma core to the plasma edge, but trapped particles are weakly affected. This observation is also confirmed by the tangential- and vertical- FIDA systems. This observation is very similar to what has been seen in conventional high field and large aspect ratio tokamaks. The observed difference in the transport of passing and trapped particles can be well explained by the pitch-dependent critical energies only under which fast ions are strongly redistributed. The standard Kadomtsev and Porcelli sawtooth models within the TRANSP code have been used to simulate the sawteeth on NSXT-U. The Kadomtsev model generally overestimates the sawtooth drops at the sawtooth crashes. When tuning the input parameters, the Porcelli model can reproduce the neutron rate drops and FIDA signal drops in the core region, but it fails to produce the FIDA signal increase at the edge. Although the TRANSP simulation with the Porcelli sawtooth model shows that passing fast ions are mainly affected by the sawtooth, this is a coincidence since the most affected region is the core region where passing particles dominate. A new sawtooth model is being developed to include energy, pitch and orbit width and will be implemented in TRANSP[37]. This new capability and more fast ion diagnostics in the coming NSTX-U run campaigns will enable more quantitative comparison between measurements and theory and help sawtooth model development and validations.

5. Acknowledgments

The authors would like to thank for the contribution of the whole NSTX-U team as well as the helpful discussions with Dr. R. Bell on CHERS data, Dr. F. Scotti on edge $D_\alpha$measurements and Dr. K. Tritz on soft x-ray data. This work is supported by the US DOE under DE-AC02-09CH11466, DE-FG02-06ER54867 and DE-FG03-02ER54681. The digital data of this paper can be found at http: //dataspace.princeton.edu/jspui/handle/88435/dsp011v53k0334

References

[1] Von Goeler S, Stodiek W and Sauthoff N 1974 *Phys. Rev. Lett.* **33**(20) 1201–1203

[2] Sauter O, Westerhof E, Mayoral M L, Alper B, Belo P A, Buttery R J, Gondhalekar A, Hellsten T, Hender T C, Howell D F, Johnson T, Lamalle P, Mantsinen M J, Milani F, Nave M F F, Nguyen F, Pecquet A L, Pinches S D, Podda S and Rapp J 2002 *Phys. Rev. Lett.* **88**(10) 105001

[3] Nielsen S K, Bindslev H, Salewski M, Brger A, Delabie E, Furtula V, Kantor M, Korsholm S B, Leipold F, Meo F, Michelsen P K, Moseev D, Oosterbeek J W, Stejner M, Westerhof E, Woskov P and the TEXTOR team 2010 *Plasma Phys. and Contr. Fusion* **52** 092001

[4] Muscatello C M, Heidbrink W W, Kolesnichenko Y I, Lutsenko V V, Zeeland M A V and Yakovenko Y V 2012 *Plasma Phys. and Contr. Fusion* **54** 025006

[5] Geiger B, Garcia-Munoz M, Dux R, Ryter F, Tardini G, Orte L B, Classen I, Fable E, Fischer R, Igochine V, McDermott R and the ASDEX Upgrade Team 2014 *Nucl. Fusion* **54** 022005

[6] Geiger B, Weiland M, Mlynek A, Reich M, Bock A, Dunne M, Dux R, Fable E, Fischer R, Garcia-Munoz M, Hobirk J, Hopf C, Nielsen S, Odstrcil T, Rapson C, Rittich D, Ryter F, Salewski M, Schneider P A, Tardini G and Willensdorfer M 2015 *Plasma Phys. and Contr. Fusion* **57** 014018

[7] Rasmussen J, Nielsen S, Stejner M, Galdon-Quiroga J, Garcia-Munoz M, Geiger B, Jacobsen A, Jaulmes F, Korsholm S, Lazanyi N, Leipold F, Ryter F, Salewski M, Schubert M, Stober J, Wagner D, the ASDEX Upgrade Team and the EUROFusion MST1 Team 2016 *Nucl. Fusion* **56** 112014

[8] Kadomtsev B B 1975 *Fiz. Plasmy* **1** 710

[9] Kadomtsev B B 1975 *Sov. J. Plasma. Phys.* **1** 389

[10] Ono M, Kaye S, Peng Y K, Barnes G, Blanchard W, Carter M, Chrzanowski J, Dudek L, Ewig R, Gates D, Hatcher R, Jarboe T, Jardin S, Johnson D, Kaita R, Kalish M, Kessel C, Kugel H, Maingi R, Majeski R, Manickam J, McCormack B, Menard J, Mueller D, Nelson B, Nelson B, Neumeyer C, Oliaro G, Paoletti F, Parsells R, Perry E, Pomphrey N, Ramakrishnan S, Raman R, Rewoldt G, Robinson J, Roquemore A, Ryan P, Sabbagh S, Swain D, Synakowski E, Viola M, Williams M, Wilson J and NSTX Team 2000 *Nucl. Fusion* **40** 557

[11] Menard J, Gerhardt S, Bell M, Bialek J, Brooks A, Canik J, Chrzanowski J, Denault M, Dudek L, Gates D, Gorelenkov N, Guttenfelder W, Hatcher R, Hosea J, Kaita R, Kaye S, Kessel C, Kolemen E, Kugel H, Maingi R, Mardenfeld M, Mueller D, Nelson B, Neumeyer C, Ono M, Perry E, Ramakrishnan R, Raman R, Ren Y, Sabbagh S, Smith M, Soukhanovskii V, Stevenson T, Strykowsky R, Stutman D, Taylor G, Titus P, Tresemer K, Tritz K, Viola M, Williams M, Woolley R, Yuh H, Zhang H, Zhai Y, Zolfaghari A and the NSTX Team 2012 *Nucl. Fusion* **52** 083015 URL `http://stacks.iop.org/0029-5515/52/i=8/a=083015`

[12] Gerhardt S, Andre R and Menard J 2012 *Nucl. Fusion* **52** 083020

[13] Ono M, Chrzanowski J, Dudek L, Gerhardt S, Heitzenroeder P, Kaita R, Menard J, Perry E, Stevenson T, Strykowsky R, Titus P, von Halle A, Williams M, Atnafu N, Blanchard W, Cropper M, Diallo A, Gates D, Ellis R, Erickson K, Hosea J, Hatcher R, Jurczynski S, Kaye S, Labik G, Lawson J, LeBlanc B, Maingi R, Neumeyer C, Raman R, Raftopoulos S, Ramakrishnan R, Roquemore A, Sabbagh S, Sichta P, Schneider H, Smith M, Stratton B, Soukhanovskii V, Taylor G, Tresemer K, Zolfaghari A and Team T N U 2015 *Nucl. Fusion* **55** 073007

[14] Menard J, Allain J, Battaglia D, Bedoya F, Bell R, Belova E, Berkery J, Boyer M, Crocker N, Diallo A, Ebrahimi F, Ferraro N, Fredrickson E, Frerichs H, Gerhardt S, Gorelenkov N, Guttenfelder W, Heidbrink W, Kaita R, Kaye S, Kriete D, Kubota S, LeBlanc B, Liu D, Lunsford R, Mueller D, Myers C, Ono M, Park J K, Podesta M, Raman R, Reinke M, Ren Y, Sabbagh S, Schmitz O, Scotti F, Sechrest Y, Skinner C, Smith D, Soukhanovskii V, Stoltzfus-Dueck T, Yuh H, Wang Z, Waters I, Ahn J W, Andre R, Barchfeld R, Beiersdorfer P, Bertelli N, Bhattacharjee A, Brennan D, Buttery R, Capece A, Canal G, Canik J, Chang C, Darrow D, Delgado-Aparicio L, Domier C, Ethier S, Evans T, Ferron J, Finkenthal M, Fonck R, Gan K, Gates D, Goumiri I, Gray T, Hosea J, Humphreys D, Jarboe T, Jardin S, Jaworski M, Koel B, Kolemen E, Ku S, Haye R L, Levinton F, Luhmann N, Maingi R, Maqueda R, McKee G, Meier E, Myra J, Perkins R, Poli F, Rhodes T, Riquezes J, Rowley C, Russell D, Schuster E, Stratton B, Stutman D, Taylor G, Tritz K, Wang W, Wirth B and Zweben S 2017 *Nucl. Fusion* **57** 102006

[15] Hawryluk R 1980 *Physics of Plasmas Close to Thermonuclear Conditionsd* vol 1 (CEC, Brussels)

[16] Pankin A, McCune D, Andre R, Bateman G and Kritz A 2004 *Comput Phys Commun* **159** 157 – 184

[17] Porcelli F, Boucher D and Rosenbluth M N 1996 *Plasma Phys. and Contr. Fusion* **38** 2163

[18] Kolesnichenko Y and Yakovenko Y 1996 *Nucl. Fusion* **36** 159

[19] Kolesnichenko Y I, Lutsenko V V, Yakovenko Y V and Kamelander G 1997 *Phys. Plasmas* **4** 2544–2554

[20] Kolesnichenko Y, Lutsenko V, White R and Yakovenko Y 2000 *Nucl. Fusion* **40** 1325

[21] Liu D, Heidbrink W W, Tritz K, Zhu Y B, Roquemore A L and Medley S S 2014 *Rev. Sci. Instrum.* **85** 11E105

[22] Liu D, Heidbrink W W, Tritz K, Fredrickson E D, Hao G Z and Zhu Y B 2016 *Rev. Sci. Instrum.* **87** 11D803

[23] Podesta M, Heidbrink W W, Bell R E and Feder R 2008 *Rev. Sci. Instrum.* **79** 10E521

[24] Bortolon A, Heidbrink W W and Podesta M 2010 *Rev. Sci. Instrum.* **81** 10D728

[25] Darrow D S 2008 *Rev. Sci. Instrum.* **79** 023502

[26] Darrow D S 2017 *Fusion Science and Technology* **71** 201–206

[27] Boeglin W U, Perez R V and Darrow D S 2010 *Rev. Sci. Instrum.* **81** 10D301

[28] Netepenko A, Boeglin W U, Darrow D S, Ellis R and Sibilia M J 2016 *Rev. Sci. Instrum.* **87** 11D805

[29] Heidbrink W W 2010 *Rev. Sci. Instrum.* **81** 10D727

[30] Hao G, Heidbrink W, Liu D, Stagner L, MPodesta, Bell R, ABortolon and Darrow D 2017 *Rev. Sci. Instrum.* **88**

submitted

[31] Cecconello M, Jones O M, Boeglin W U, Perez R V, Darrow D S, Klimek I, Sharapov S E, Fitzgerald M, McClements K G, Keeling D L, Allan S Y, Michael C A, Akers R J, Conway N J, Scannell R, Turnyanskiy M, Ericsson G and the MAST Team 2015 *Plasma Phys. and Contr. Fusion* **57** 014006

[32] Graves J P, Chapman I T, Coda S, Johnson T, Lennholm M, Paley J I, Sauter O and Contributors J E 2011 *Fusion Science and Technology* **59** 539–548

[33] Heidbrink W, Liu D, Luo Y, Ruskov E and Geiger B 2011 *Comm. Comp. Phys.* **10** 716–741

[34] Yakovenko Y V, Kolesnichenko Y I, Lutsenko V V, Burdo O S and White R B 2006 *2006 Proc. 24th IAEA Fusion Energy Conf.* (Chengdu, China) pp TH/P6–6

[35] Kolesnichenko Y I, Lutsenko V V, White R B and Yakovenko Y V 1998 *Physics of Plasmas* **5** 2963–2976

[36] Kolesnichenko Y I, Lutsenko V V and Yakovenko Y V 1998 *Phys. Plasmas* **5** 729–734

[37] Kim D, Podesta M, Liu D and Poli F M 2017 *Nucl. Fusion* **57** submitted

Figures

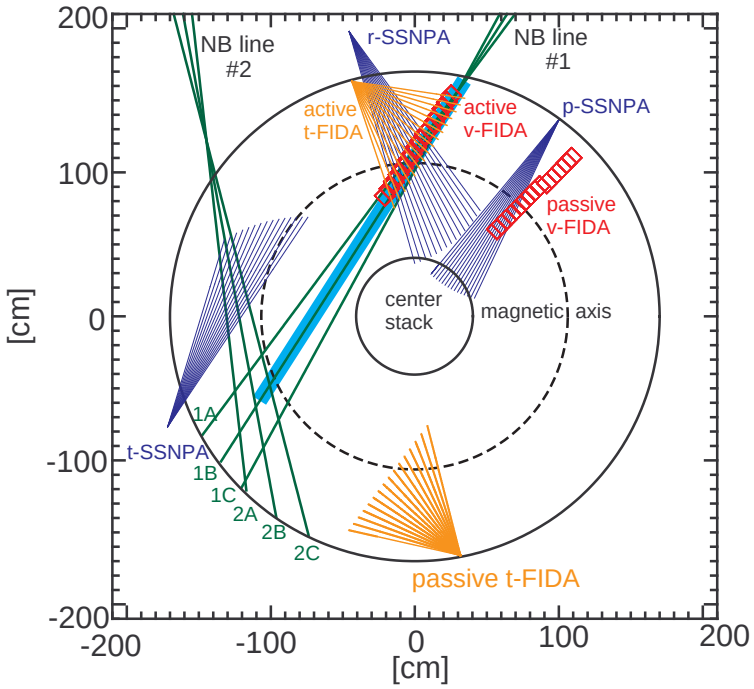

Figure 1. (Color online) Plan view of the NSTX-U vessel with neutral beam centerlines, tangential- and vertical- FIDA sightlines, tangential-, radial- and passive- SSNPA sightlines. The original NSTX beams are labeled $1A$, $1B$ and $1C$, and the new added three beam sources are label $2A$, $2B$ and $2C$. In most discharges analyzed in this paper, only the neutral beam source 1B is used, and the shaded light blue region represents the nominal beam width. The normal directions for the plasma current and toroidal field are counter-clockwise and clockwise, respectively.

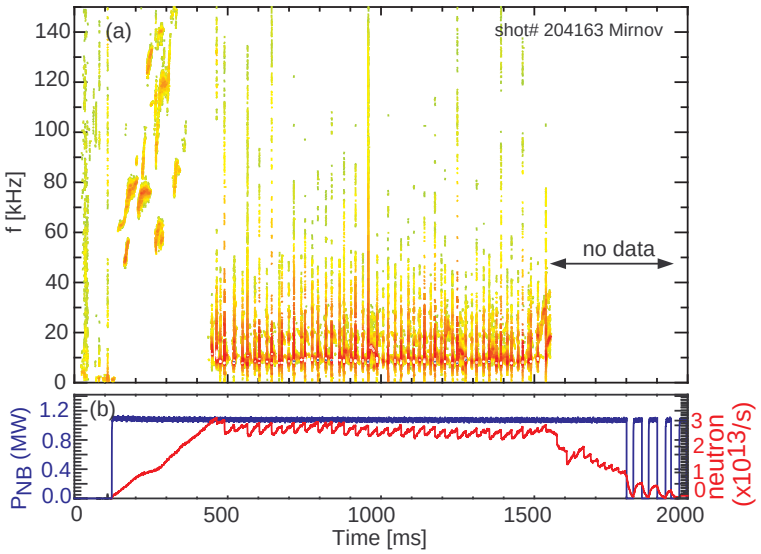

Figure 2. (Color online) (a) Spectrogram of Mirnov coil signal and (b) temporal evolution of neutron rate and neutral beam injection power. Repetitive sawtooth crashes occur between 0.5 and 1.5 s.

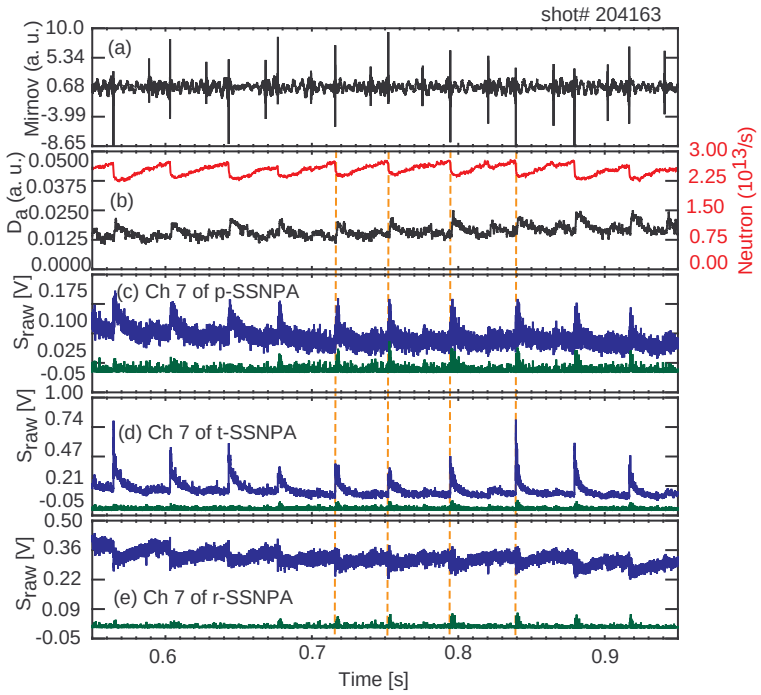

Figure 3. (Color online) Temporal evolution of (a) Mirnov coil signal, (b) neutron emission and $D_\alpha$radiance from the edge of the plasma, (c) signal of channel 7 of passive-SSNPA, (d) signal of channel 7 of tangentially-viewing SSNPA and (e) signal of channel 7 of radially-viewing SSNPA. In each detector array, one detector is blocked as a ”blind” detector to monitor EM noise and neutron induced noise. The signals on those ”blind” detectors are also shown in green curves in (c)-(e) .

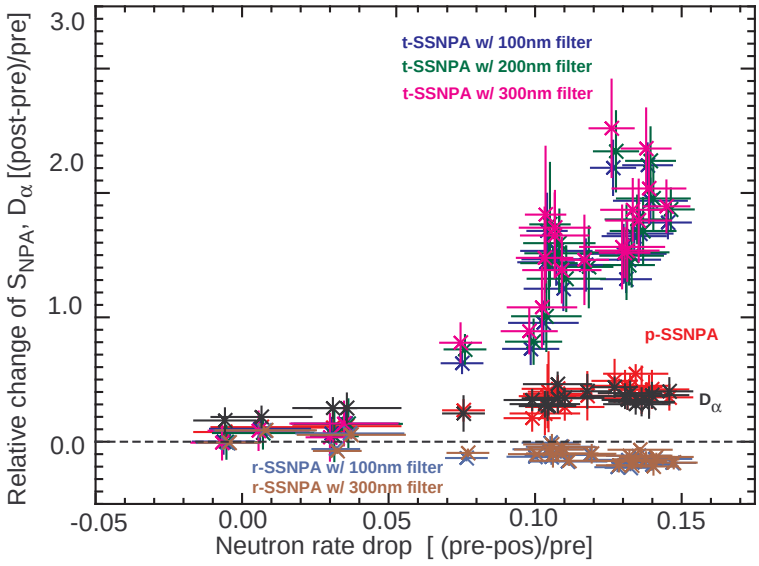

Figure 4. (Color online) Relative change of edge D_α and SSNPA signals vs the neutron rate drop at the sawtooth crashes. For the tangentially-viewing and radially-viewing SSNPA instruments, each instrument has three arrays with directly deposited foils of different thickness. The corresponding energy threshold for 100 nm, 200 nm and 300 nm filters are $>$ 25 keV, $>$ 45 keV, and $>$ 65 keV respectively. In the discharge 204163, the data were only available for two arrays of r-SSNPA due to lack of amplifiers for the third array at that time. The error bar of the neutron rate drop represents the statistical error of neutron measurements, while the error bar of SSNPA signals is calculated with the noise observed on the "blind" detector.

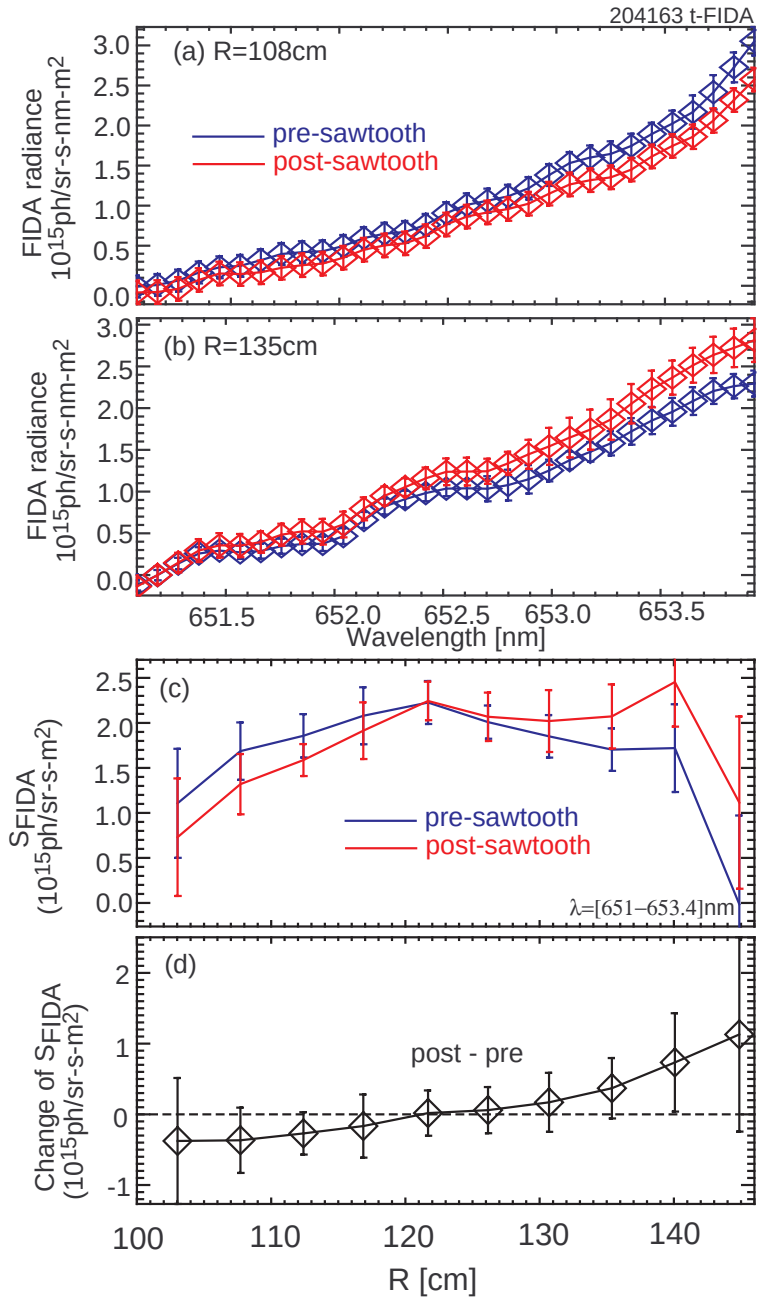

Figure 5. (Color online) Comparison of t-FIDA spectra before and after the sawtooth crash for (a) a core channel with $R_{maj} = 108$ cm and (b) a edge channel $R_{maj} = 135$ cm. (c) Comparison of t-FIDA spatial profiles before and after the sawtooth crash. (4) Relative change of t-FIDA radiance before and after the sawtooth crash. Note the FIDA data are conditional averaged over several sawtooth events.

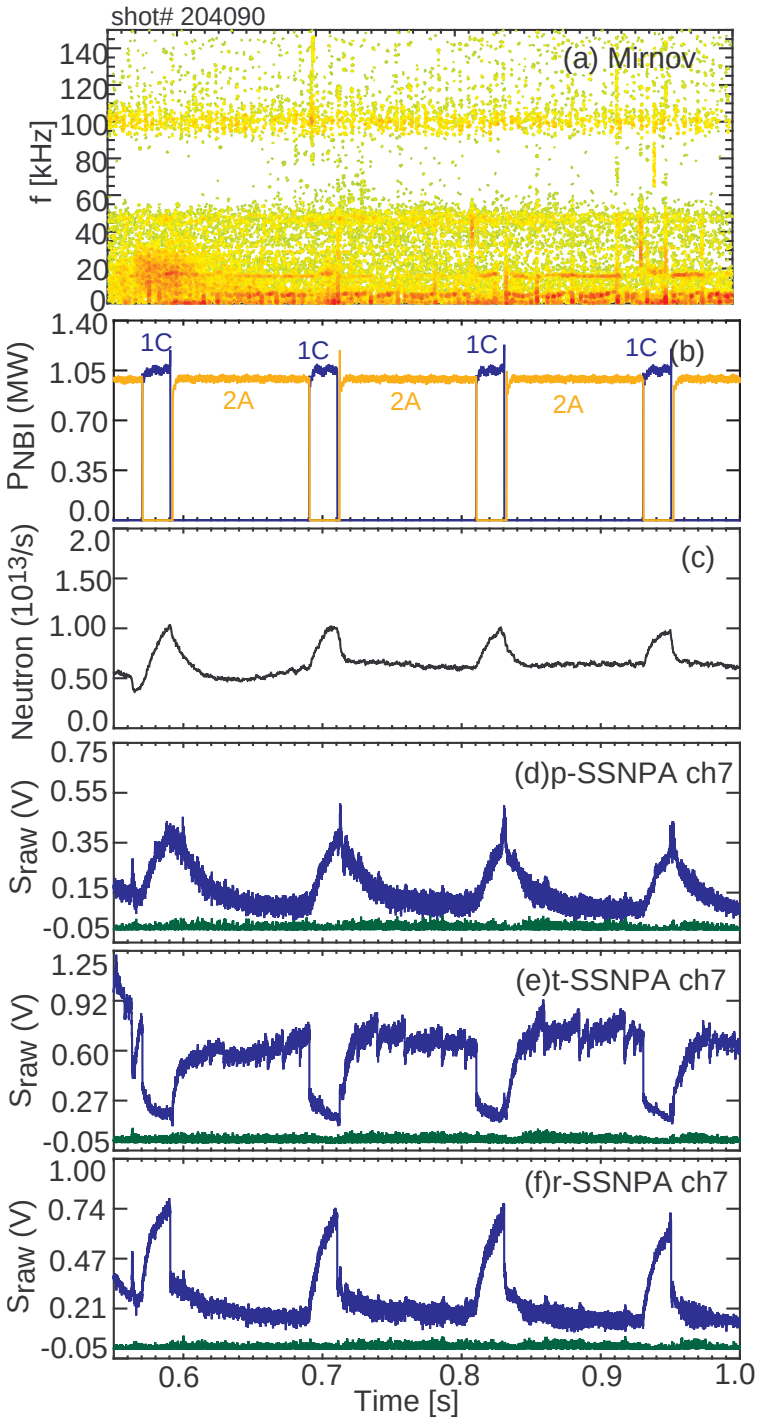

Figure 6. (Color online) (a) Spectrogram of Mirnov coil signals. Temporal evolution of (b) injected neutral beam power, (c)neutron emission, (d)signal of channel 7 of passive-SSNPA, (e)signal of channel 7 of tangentially-viewing SSNPA and (f) signal of channel 7 of radially-viewing SSNPA. The signals on those "blind" detectors are also shown in green curves in (d)-(f) to represent the typical noise level.

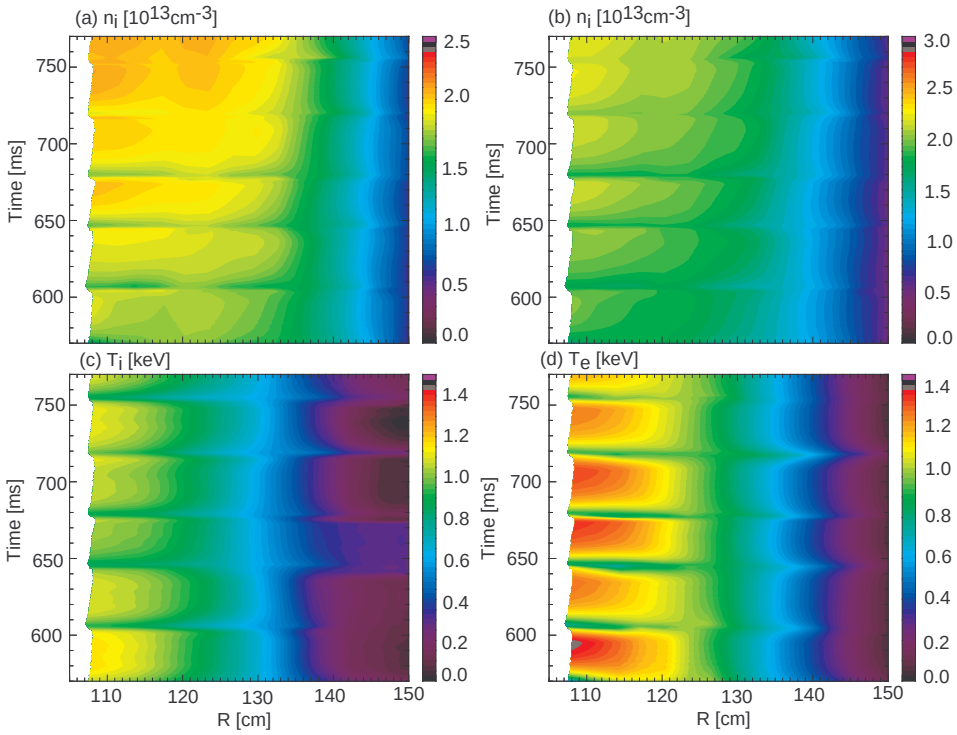

Figure 7. (Color online) Temporal evolution of profiles of (a) thermal ion density, (b) thermal electron density, (c) ion temperature, and (d) electron temperate. These profiles are obtained by conditionally averaging over all sawtooth events between 0.5 and 1.5s and are re-sampled on 1 ms time intervals. They are used as input plasma profiles for TRANSP sawtooth simulations.

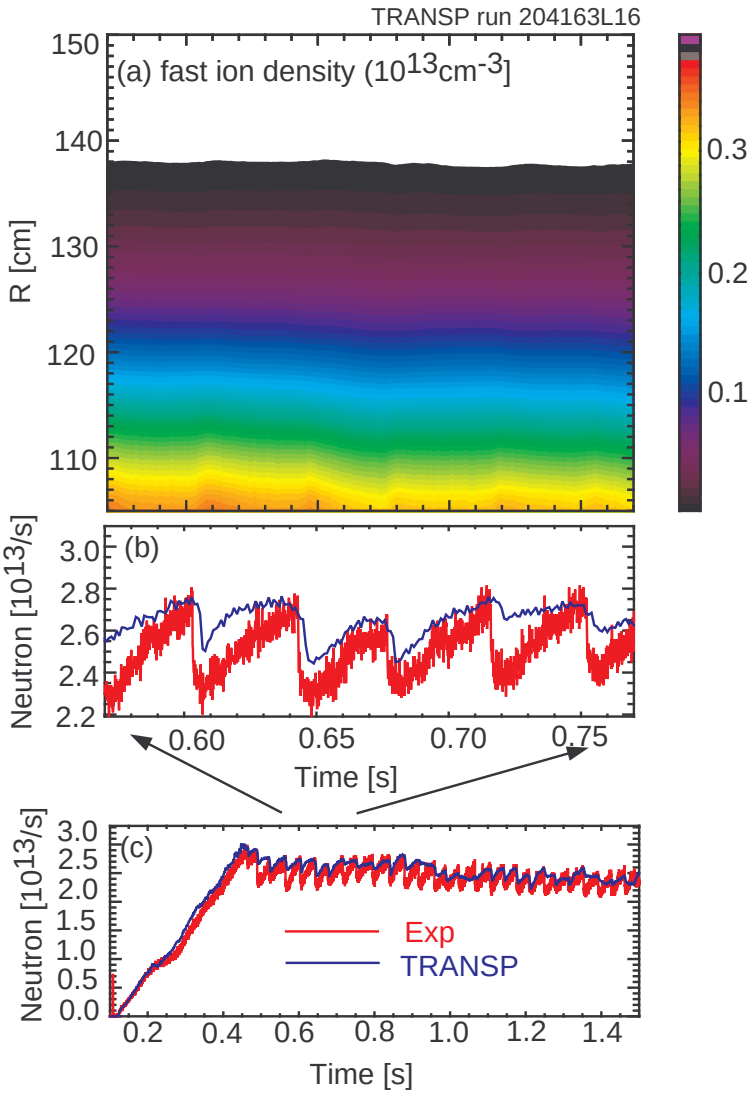

Figure 8. (Color online) (a) Fast ion density and (b,c) neutron emission calculated by TRANSP simulation $204163L16$ in which sawtooth model is turned on for q profile evolution, but it is turned off for fast ions. The measured neutron rate is shown red curve in panel (b) and (c) for comparison. The TRANSP simulation predicts that the neutron rate drop caused by thermal plasma profile evolution can be as much as 50% of the measured neutron rate drop at the sawtooth crash.

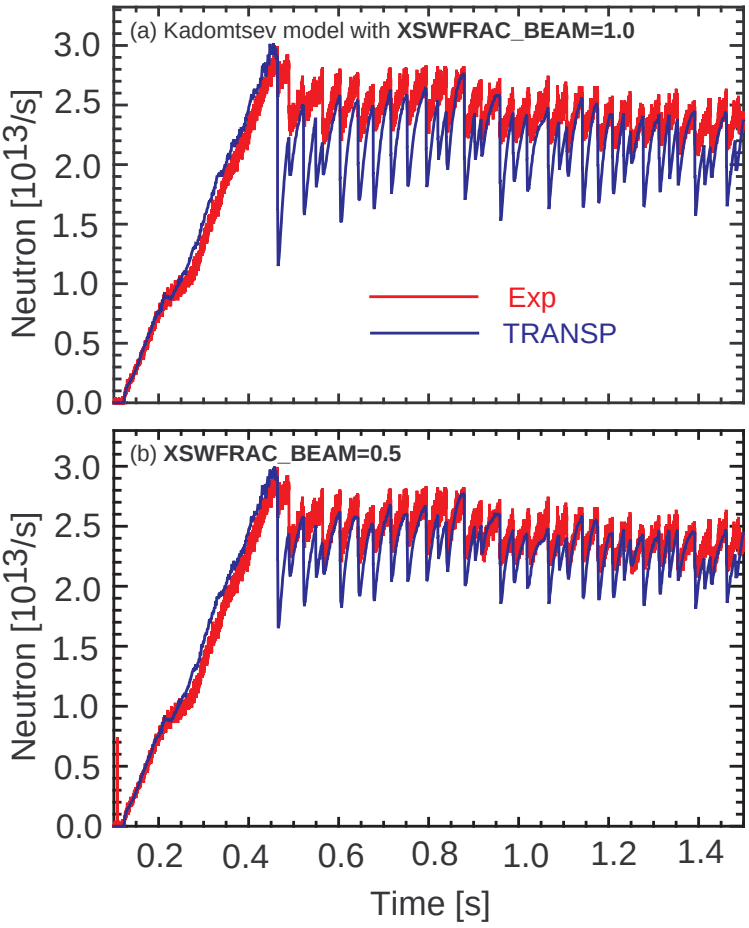

Figure 9. (Color online) TRANSP/NUBEAM calculated global neutron emission compared with the measured neutron rate. The standard Kadomtsev sawtooth model is employed in these TRANSP/NUBEAM simulations with (a)$XSWFRAC\_BEAM = 1.0$ and (b) $XSWFRAC\_BEAM = 0.5$, where $XSWFRAC\_BEAM$ is the fraction of fast ions participating in sawtooth mixing. The standard Kadomtsev sawtooth model overestimates the neutron rate drop at the sawtooth crash.

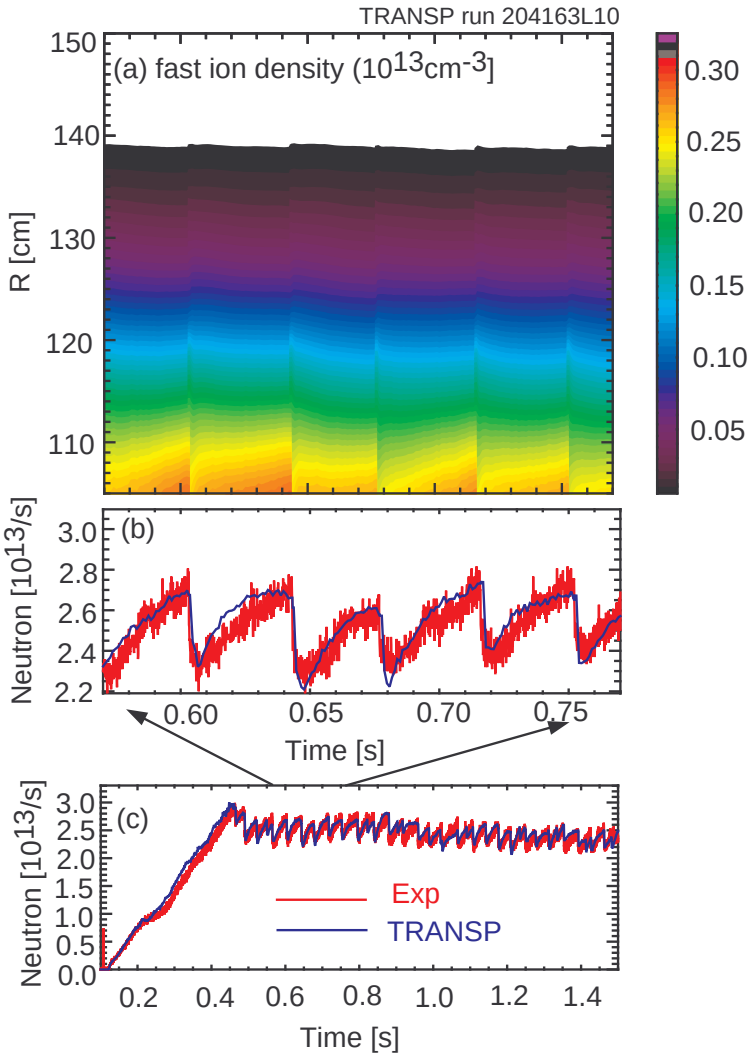

Figure 10. (Color online) (a) Fast ion density and (b,c) neutron emission calculated by TRANSP simulation $204163L10$ with Porcelli sawtooth model. The measured neutron rate is also shown red curve in panel (b) and (c) for comparison. The predicted neutron emission and neutron drops at the sawtooth crashes can reasonably agree with the measurement.

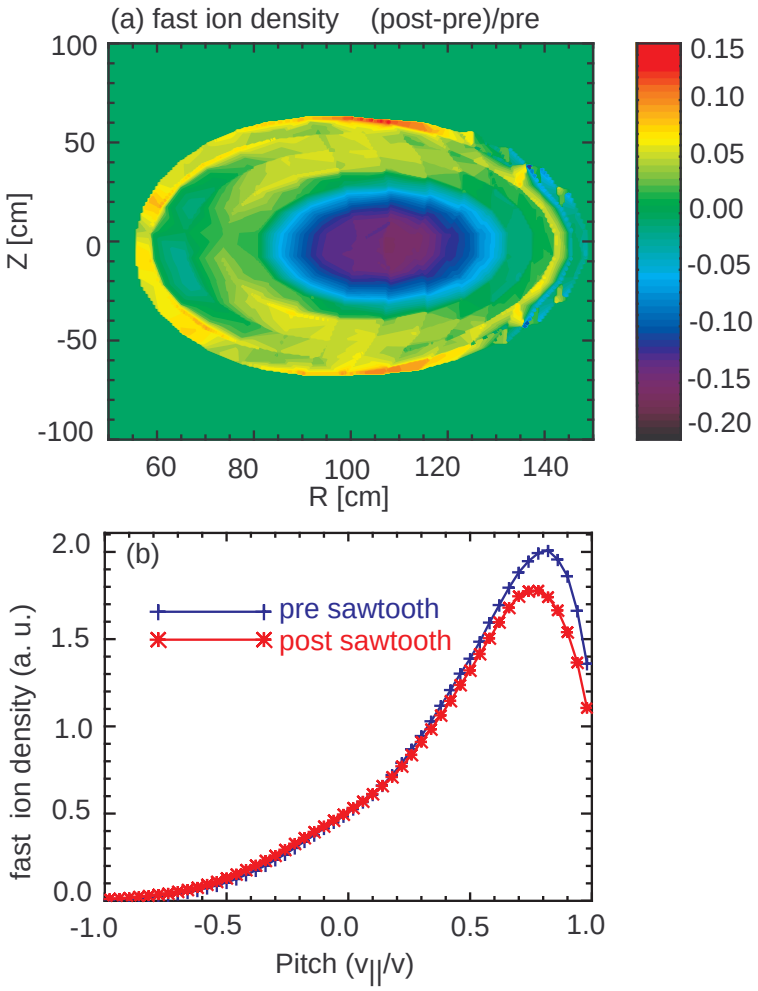

Figure 11. (Color online) Difference of fast ion distribution function before and after the sawtooth crash in (a) (R, Z) space and (b) pitch ($V_{||}/v$) relative to plasma current.

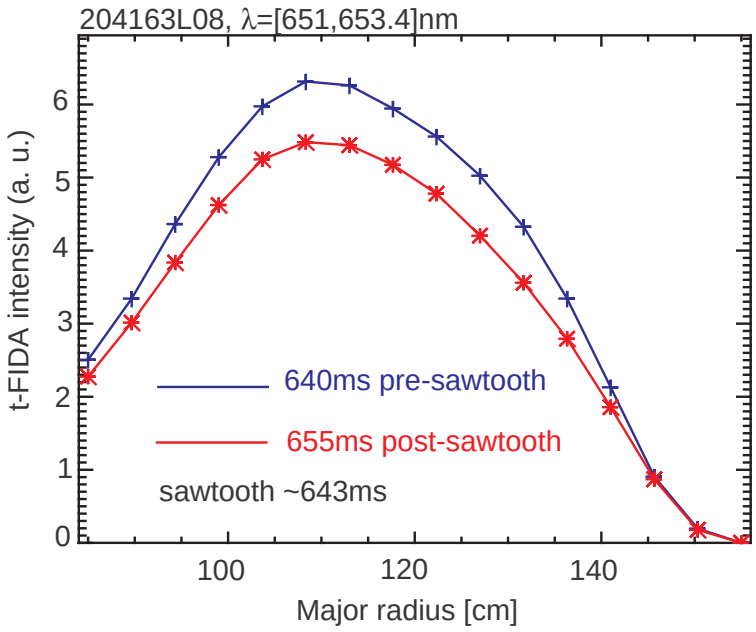

Figure 12. (Color online) Comparison of simulated t-FIDA spatial profiles before and after the sawtooth. The synthetical t-FIDA signal is calculated by FIDAsim using the plasma profiles and fast ion distribution from TRANSP with the Porcelli sawtooth model. The t-FIDA spectra are integrated over [651,653.4] nm, whose corresponding energy range is [15, 60] keV, to get the t-FIDA spatial profile.